Photocatalysis in Gold Nanocage Nanoreactors†

C. W. Yen, M. A. Mahmoud, and M. A. El-Sayed*

Laser Dynamics Laboratory, School of Chemistry and Biochemistry, Georgia Institute of Technology, Atlanta, Georgia 30332-0400

Received: December 13, 2008; Revised Manuscript Received: January 15, 2009

The photodegradation of methyl orange was found to take place very efficiently using hollow Au nanocages which are known to have remaining Ag on their interior walls which can be oxidized to Ag_2O. The degradation rate is found to be more efficient than photodegradation reaction using semiconductor nanomaterials, such as TiO_2 and ZnO. The reaction rate is found to increase by increasing the degree of Ag oxidation on the interior wall of the nanocages prior to the reaction and is a function of the nanocavity size and the pore density of the nanocage walls. As the cage size varies, it is found that the photocatalytic rate increases and then decreases with a maximum rate at nanoparticle size of 75 nm with a medium pore density in the walls. All these results suggest that the catalysis is occurring inside the cavity, whose interior walls are covered with the Ag_2O catalysts. Similar to the mechanism proposed in the degradation by the other semiconductors, we propose that the photodegradation mechanism involves the formation of the hydroxyl radical resulting from the photoexcitation of the Ag_2O semiconductor. The observed results on the rate are discussion in terms of (1) the surface area of the inner wall covered with Ag (Ag_2O), (2) the density and size of the pores in the walls, and (3) the cavity size of the nanoparticles.

1. Introduction

Nanomaterials with hollow structure are promising, due to their unique optical and catalytical properties.[1−7] Due to the larger surface to volume ratios, they are expected to be more effective in catalysis. Gold nanocages were first synthesized by Xia et al.[8] They have developed a facile way to synthesize nanoparticles of uniform shape and size with hollow interiors and have demonstrated that hollow nanocages have high catalytic activity, similar to Pd nanotubes for the Suzuki coupling reaction[9] and Pd−Au−Ag nanocages for methyl red hydrogenation.[10] Hollow gold nanocages that are very stable and have a novel layered structure have never been used as a novel photocatalyst.[11] In this work we used them in the photodegradation of methyl orange (MO) dye and found them to be more efficient than TiO_2[12−14] and ZnO[15] in the photodegradation of azo dyes.

The most common reported photocatalyst for the photocatalytic oxidative degradation of azo dyes is semiconductor materials, such as TiO_2[12−14] and ZnO.[15] The basic photocatalytic principle of semiconductor materials (usually metal oxides) is photogenerated electrons (from the conduction band) and holes (from the valance band) migrating to the metal oxide surface and reacting with adsorbed O_2/H_2O to generate reactive radicals which can attack the azo dyes and lead to their photodegradation.[12]

The method of galvanic replacement transforms the silver nanocubes into gold nanocube shells with pores in the walls whose number increases with the nanocube shell size, and their inside wall are coated with the remaining silver. In the present work, we examine the effect of cavity size on the rate of the photodegradation of the methyl orange dye by using the Ag walls of the Au nanocavity. It is known that silver is easily oxidized to silver oxide solution even at 300 K, and the formation of silver oxide (Ag_2O) is extremely stable in ambient conditions.[16] The reported band gap of silver oxides is ∼2.5 eV (400−500 nm), and it can therefore be analogous to the other semiconductor materials.[17] Upon the absorption of the light energy, it produces radicals that could perform oxidative degradation of MO.

We prepared gold nanocages of various sizes and different cavity volumes to serve as nanoreactors. The photodegradation reaction of MO demonstrates that the oxygen treatment is the key point for nonreactors to become a good photocatalyst for this reaction. We found that the catalytic activity increases and then decreases as the nanocavity becomes larger. This is explained by the fact that increasing the cavity size first increases and then decreases the cavity surface area. The smaller surface area at the large cavity is proposed to result from the increase in its surface pores.

2. Experimental Section

Gold nanocages (AuNCs) of various sizes and wall thicknesses were prepared from silver nanocube template nanoparticles via the galvanic replacement method.[18] Silver nanocubes (AgNCs) were prepared by heating 30 mL of ethylene glycol (EG) at 150 °C for 1 h, followed by the addition of 0.2 g of poly(vinylpyrrolidone) (PVP, MW 55k) dissolved in 10 mL of EG. The resulting solution was heated until the temperature reached 150 °C. A solution of 0.4 mL of sodium sulfide dissolved in ethylene glycol (3 mM) was added. Three sizes of AgNCs were prepared (50, 75, and 100 nm) by slowly injecting various amounts of silver nitrate (2.5, 3, and 3.5 mL of 282 mM dissolved in EG, respectively) into the reaction mixture. The silver ions were reduced completely after 15 min, producing AgNCs. Diluting 10 mL of AgNC solution with acetone and subsequently centrifuging purified the AgNCs. The particles were then redispersed in deionized water. The solution of purified AgNCs was brought to a boil, and a 10 mg/L solution

† Part of the "George C. Schatz Festschrift".

* Author to whom correspondence should be addressed. E-mail: mostafa.el-sayed@chemistry.gatech.edu.

10.1021/jp811014u CCC: $40.75
Published on Web 03/09/2009

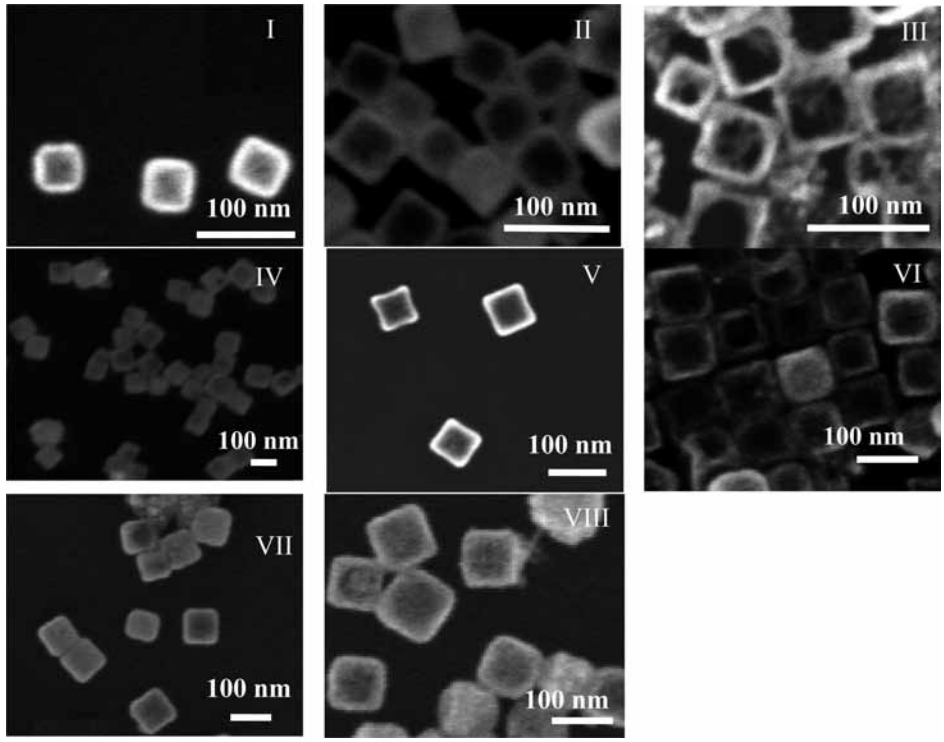

Figure 1. SEM images of AuNC samples. I, II, and III are the 50 nm AuNCs. IV, V, and VI are the 75 nm AuNC samples. VII and VIII are the 100 nm AuNC samples. I, IV, and VII are the boxlike AuNCs. II, V, and VIII are the porous AuNCs. III and VI are the framelike AuNCs.

of hydrogen tetrachloroaurate was injected slowly. This mixture was continuously refluxed until its color remained constant. Vigorous magnetic stirring was maintained throughout the synthesis. The thickness and porosity of the AuNCs' walls were controlled by the amount of gold salt added to the solution.[19] Eight individual colloidal solutions of AuNCs were prepared from the three sizes of AgNCs (50, 75, and 100 nm). From the 50 nm AgNCs, three AuNC samples were synthesized of different wall thickness (samples I, II, and III). From the 75 nm AgNCs, three AuNC samples were synthesized of different wall thickness (samples IV, V, and VI), and from the 100 nm AgNCs, two samples were synthesized of different wall thickness (samples VII and VIII). As the shape of the nanocages was varied through additional $AuCl_4^-$, the surface plasmon resonance was red-shifted, due to the further loss of silver atoms in the alloy structure. Oxygen treatment of the AuNCs was performed prior to the photocatalysis experiments. An aliquot of 50 mL of the AuNC solution was stirred in the cylinder, and oxygen gas was bubbled through the solution at a rate of 30 mL/min for 6 h to oxidize the silver atoms of the AuNCs to silver oxide (Ag_2O). The photocatalysis reactions were carried out in a quartz cell containing the reaction mixture irradiated by a 50 W high-pressure Xe−Hg lamp (the light intensity near the solution surface was about 120 mW/cm^2). The reaction temperature was held constant at room temperature to reduce thermal effects on the catalytic rate. The reaction mixture was composed of 2 mL of the nanocube solution and 200 μL of methyl orange (MO) (20 mg/ L). Optical measurement of the characteristic peak of MO (~480 nm) was used to monitor the changes in the concentration of the MO reactant during the photocatalytic experiments. All optical measurements were collected using an Ocean optics UV−vis spectrometer HR4000Cg-UV−NIR.

The 50 nm AuNCs with surface plasmon peaks at 650, 700, and 800 nm had optical densities (ODs) of 1.5, 2.6, and 2, respectively. The 75 nm AuNCs had ODs of 1.8, 2.3, and 2, respectively. The 100 nm AuNCs with plasmon peaks at 700 and 800 nm had ODs of 1.5 and 1.4, respectively. A Holoprobe Raman microscope (Kaiser Optical Systems) with 785 nm laser excitation was used for Raman measurements.

3. Results and Discussion

To prepare various sizes of AuNCs, one must synthesize AgNCs first for use as a sacrificial template during the galvanic replacement reaction. Here, three different sizes of AgNCs were prepared (50, 75, and 100 nm). The synthetic approach of AuNCs is based on the galvanic replacement reaction between AgNCs and the gold salt solution. The gold ions are reduced at the expense of silver atoms that compose the nanocubes, which are oxidized via the following equation:[19]

$$3Ag_{(s)} + AuCl_{4(aq)}^- \rightarrow Au_{(s)} + 3Ag_{(aq)}^+ + 4Cl_{(aq)}^- \quad (1)$$

The first stage of this synthesis is a solid silver−gold alloy wall formed when a relatively small amount of gold salt is added to the template solution. Their boxlike and solid Au/Ag alloy wall characterizes the particles in this stage, and the SEM images show the uniformity and closed wall structures (See Figure 1, I, IV, and VII).[18−20] In the later stage of synthesis, as more gold salt is added to the boxlike AuNC solutions, some silver atoms undergo a dealloying process from the Au/Ag alloy walls. Numerous pores within the walls are formed by selectively extracting silver atoms, and porous AuNCs are generated from the boxlike AuNCs. The continuous etching of the silver core leads to an increase in the void size and causes the SPR peak to red-shift compared to the corresponding solid boxlike AuNC structure (Figure 2). In the final stage of synthesis, when the amount of gold salt added to the porous AuNCs was further increased, Au atoms were simultaneously reduced, inducing changes in the porosity. According to eq 1, one gold cation

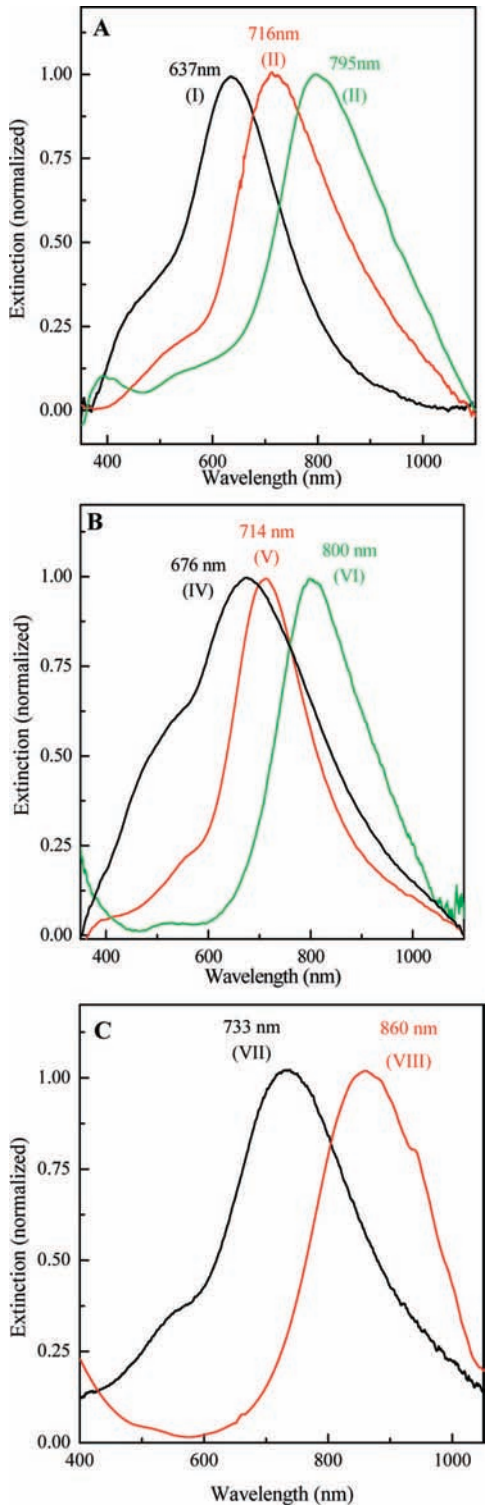

Figure 2. Normalized SPR extinction spectra of (A) 50 nm size AuNCs, (B) 75 nm size AuNCs, and (C) 100 nm size AuNCs. By varying the volume of $HAuCl_4$ solution added to the AgNCs, the SPR band of the AuNCs was tuned from the visible to the near-IR region due to changes in porosity and volume of the cavity of the particles. The particles are divided into three groups: (1) poreless Au/Ag alloy walls, boxlike AuNCs (samples I, IV, and VII), (2) enlarged pores in the Au/Ag alloy walls, porous AuNCs (samples II, V, and VIII), and (3) nearly empty interiors, framelike AuNCs (samples III and VI).

(Au^{3+}) is reduced by three silver atoms, thus resulting in a continuous etching of the silver core producing nearly an empty AuNC (Figure 1, III and VI). Because of the loss of the silver atoms, AuNCs in the final stages were transformed into framelike AuNCs producing vacant cavities of AuNCs. Increasing the pore sizes in the walls and thinning the wall thickness caused a shift in the SPR peak of the framelike AuNCs from the visible to the near-IR range (800 nm, Figure 2A, B). In summary, the synthetic steps based on galvanic replacement are a simple and versatile method to make gold nanostructures with a specific porosity of the wall, a precise volume of the cavity, and a desired position of the SPR band.[18−20]

To activate the AuNCs as photocatalysts, the remaining silver atoms on the inside walls of the cavity of the AuNCs were oxidized into silver oxides (Ag_2O). The silver oxide is capable of adsorbing the energy from light at a frequency between 400 and 500 nm to produce radicals that perform oxidative degradation of azo dyes. Silver atoms can be efficiently converted into silver oxides upon oxygen treatment by bubbling oxygen gas into the solution. The oxidation of silver into silver oxide by oxygen gas is thermodynamically and electrochemically allowed at room temperature.[16,21] Oxygen gas oxidizes silver atoms according to the following equation:

$$\begin{array}{ll} 4Ag + 2H_2O \rightarrow 2Ag_2O + 4H^+ + 4e^- & E^o = -1.173\ V \\ \underline{O_2 + 4H^+ + 4e^- \rightarrow 2H_2O} & \underline{E^o = +1.229\ V} \\ 4Ag + O_2 \rightarrow 2Ag_2O & \Delta E = +0.056\ V \end{array}$$

Figure 3A shows the surface plasmon spectra of AuNCs before and after oxygen treatment. The surface plasmon resonance red-shifts upon oxidation, which is in agreement with the results of other groups.[22−24] In addition, the comparison of the Raman spectra of the fresh and oxygen-treated AuNCs shows a large increase in the silver oxide (Ag_2O) peak at 525 cm^{-1} in oxygen-treated samples (Figure 3B).[25,26]

The AuNCs performed well as photocatalytic degradation on the MO agents after being activated through oxygen treatment. Prior to oxygen treatment, the AuNCs lacked photocatalytic activity in the catalytic degradation of MO. The change in MO concentration was quantitatively monitored during the reaction by monitoring the optical absorption peak intensity located around 480 nm. This peak is sensitive to the changes in pH of the medium and red-shifts with decreasing pH. In the absence of the photocatalyst, the MO itself is stable for several hours upon irradiation with the Xe−Hg lamp (data not shown). Therefore, the observed rapid decrease of the MO absorbance peak in the presence of AuNCs results from the catalyzed photodegradation. The absorbance intensity at 480 nm of MO is measured in intervals of 10 min, and the reaction rate was obtained by calculating the absorbance change of MO as a function of time.

The photocatalytic activities of three different sizes of AuNCs (50, 75, and 100 nm) having the same SPR band position (around 700 nm) under the same conditions were compared. During the 60 min photocatalytic reactions, the photodegradation process of MO was almost complete when catalyzed by 75 nm AuNCs (Figure 4B). However, 30% and 60% of the MO remained when the degradation catalysis was carried out by the 50 and 100 nm AuNCs, respectively (Figure 4A and C). All eight AuNCs samples synthesized here were used as photocatalysts, and their activities were studied. The reaction rates of these eight catalysts all obeyed first-order kinetics as shown in parts A, B, and C of Figure 5. The time-dependent extinction spectra of MO catalyzed by only three samples are shown in Figure 4.

The photocatalytic abilities of AuNCs and solid AgNCs were compared. There is no hollow cavity inside the AgNCs because

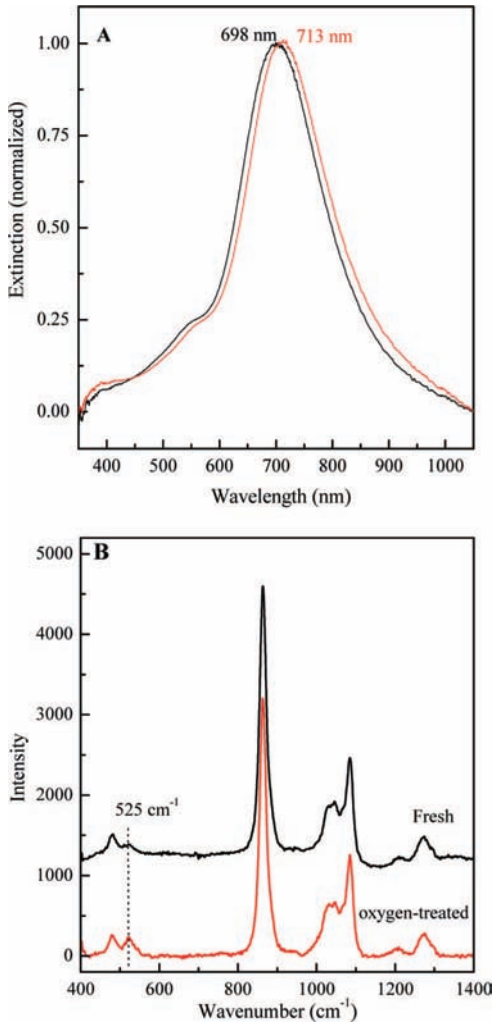

Figure 3. (A) Surface plasmon resonance spectra of 75 nm AuNCs before (black) and after (red) treatment with oxygen gas. (B) Raman spectrum of AuNCs before (black) and after (red) oxygen treatment. Shift in surface plasmon spectrum and the increases in intensity of the 525 cm^{-1} Ag_2O Raman band both support the formation of Ag_2O by oxygen treatment.

they are solid nanostructures. For AgNCs (fresh and oxygen treated ones), the photocatalytic activity was significantly nonexistent, as indicated by no measurable change in the MO absorption peak during the reaction. Although the absorption peak of MO and the SPR band of pure AgNCs were close to one another, the change of the MO absorption peak can still be monitored during the photocatalytic reactions. During the 1 h reaction time, there was only a slight change of the MO absorbance (results not shown).

There are a number of observations that strongly suggest that the catalysis occurs within the cage cavity of these particles: (1) the observation that oxidized Ag (which is only present on the inside walls of the cavity) is required for the catalytic process, (2) the dependence of the catalytic rate on the cavity size, and (3) the fact that solid Ag cubes have no significant catalytic activity.

The photocatalytic activity of the three classifications of AuNCs (boxlike, porous, and framelike) can be distinguished from one another. Among these three different categories, the most inactive one is the boxlike AuNCs (samples I, IV, and VII) and the most active one is the porous AuNCs (samples II, V, and VIII). The rate constants for the photodegradation of MO by samples I, IV, and VII (boxlike) were found to be 0.002,

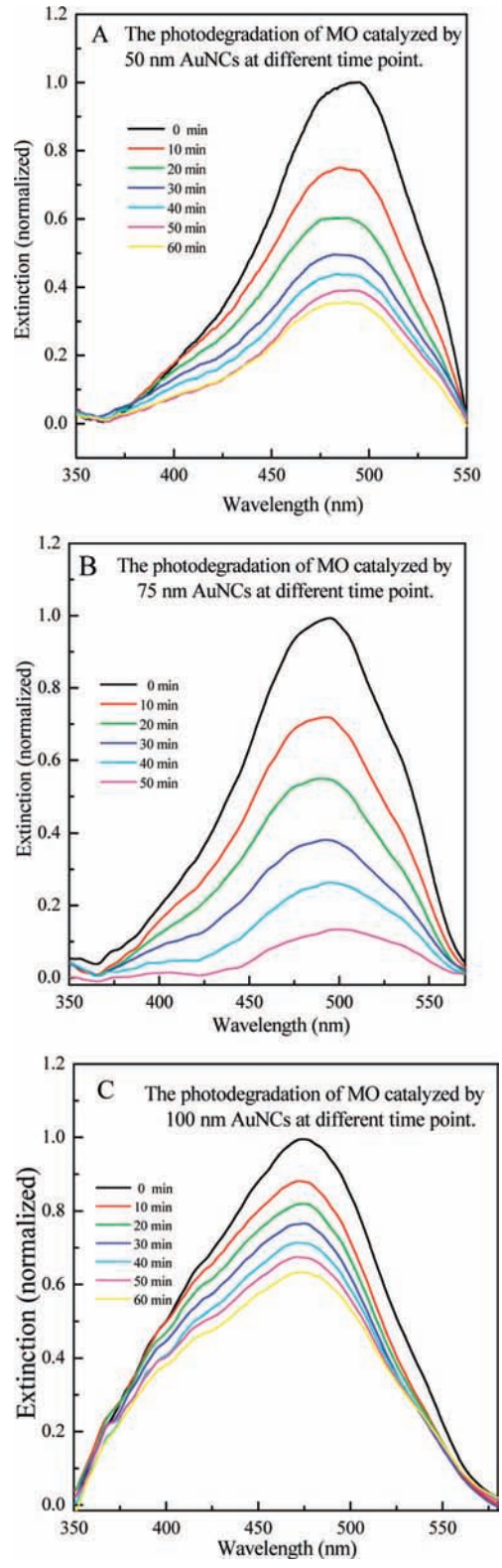

Figure 4. Time-dependent extinction spectra of methyl orange catalyzed by AuNCs with similar SPR bands at 700 nm but of different sizes: (A) 50 nm (sample II), (B) 75 nm (sample V), and (C) 100 nm (sample VII). The photodegradation experiment took 1 h, and absorbance of MO was measured every 10 min. All three experiments were performed under the same conditions.

0.002, and 0.007 min^{-1} of cage sizes of 50, 75, and 100 nm, respectively (slope of black data points in Figure 5). The rate constants for the photodegradation of MO by samples II, V, and VIII (porous) were all far beyond 0.010 min^{-1} (slope of

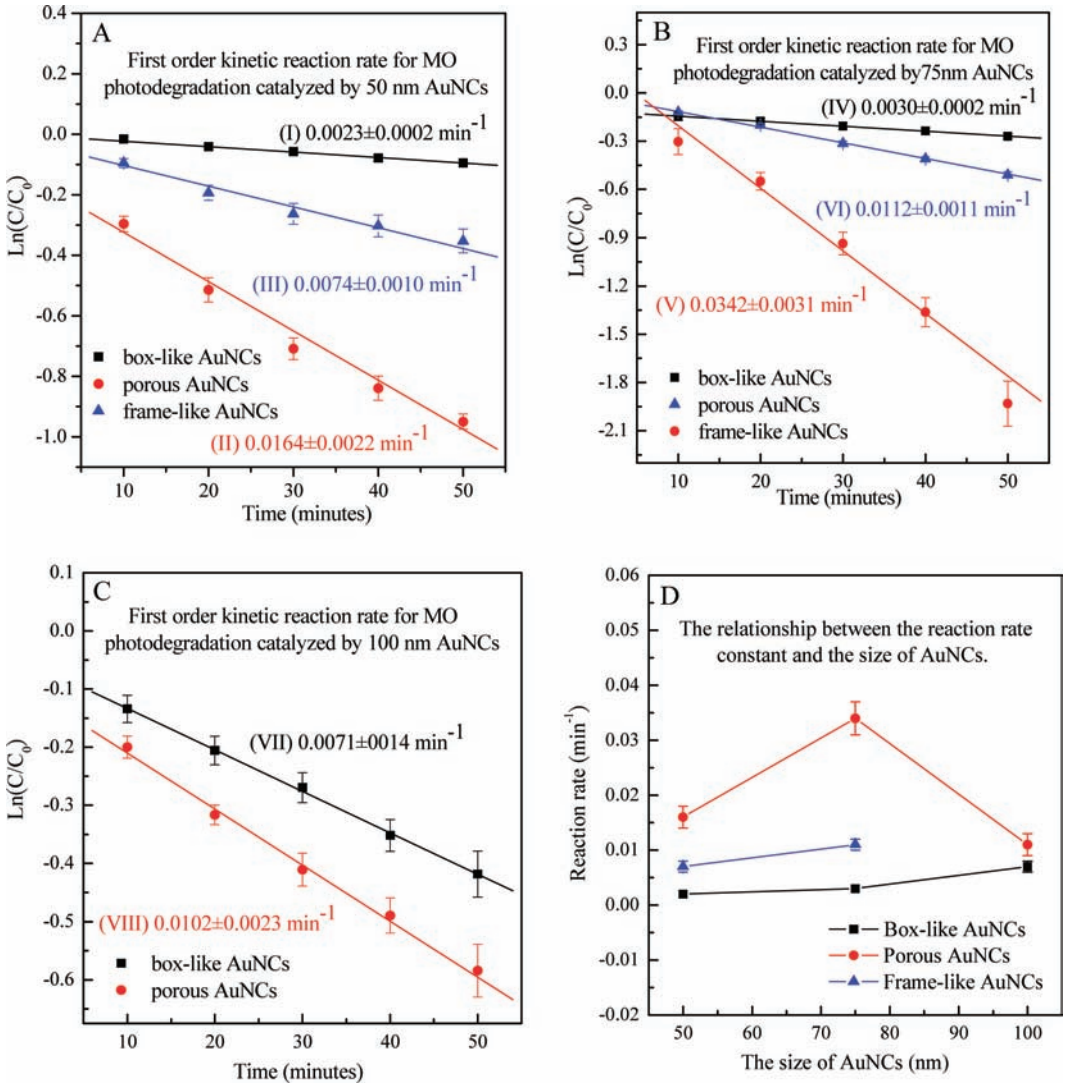

Figure 5. First-order relationship for the photocatalytic degredation of methyl orange by AuNCs of different cage sizes: (A) 50, (B) 75, and (C) 100 nm. Three different colors represent different groups of AuNCs: black is the boxlike AuNCs, red is the porous AuNCs, and blue is the framelike AuNCs. (D) The correlation between the size of AuNCs and the reaction rate and the comparison of three different kinds of AuNCs.

the red data points in Figure 5), with the highest rate of 0.034 min^{-1} for the 75 nm size porous cages (sample V). The reaction rate constants of framelike AuNCs (slope of the blue data points in Figure 5) were all in between the boxlike and porous AuNC rates.

4. Possible Mechanism

Upon excitation of silver oxide above the band gap energy, electrons are excited from the valence band to the conduction band, generating a hole in the valence band. Water molecules in the solution are oxidized into hydroxyl radicals and protons by the holes in the valence band,[27,28] while the electrons in the conduction band reduce oxygen in the presence of water molecules into hydroxyl and peroxide radicals. Those generated radicals react with the MO molecules, resulting in MO radicals, and MO radicals undergo a series of intramolecular fragmentation. It is necessary to continuously produce hydroxyl radicals to continue the photodegradation reactions. The hydroxyl radical generation process is depicted in Figure 6A and B.

There are three factors affecting the rate of the reaction. The first factor is the surface area of the Ag_2O covered wall inside the cavity. Since the inner walls of the AuNCs are coated with Ag_2O, the hydroxyl radicals are generated on the inner surface of the cavity. The increased surface area inside the cavity of the particle contributes to the increase in the concentration of the hydroxyl radical as well as an increase in the collision probability. The second factor is the pore size of the AuNCs. The pore size in the wall of the cage could affect the rate of the photocatalytic reactions. The reactant dyes and the product photofragments diffuse in and out through the pores of the cage. Thus the pore size on the particle walls serves to regulate the flux of molecular species and thus maintains the steady state concentration during the reaction. The third factor is the size of the cage in which the hydroxyl radicals and the MO collide with each other. The cavity size thus controls the collision rate between the hydroxyl radicals and the MO dye molecules.[29]

There are three different cube sizes of AuNCs, and the cavity sizes can be controlled by adding various amounts of gold salt. For the particles with the smallest cavity, the boxlike AuNCs (samples I, IV, and VII), the reaction rate of all three sizes are the slowest (under 0.007 min^{-1}). Previously it was mentioned that the most significant reason for the low activity of boxlike AuNCs is because they lack pores in their walls. The dye molecules could not diffuse easily and rapidly due to the poreless walls of boxlike AuNCs. This means the reactants could not be catalyzed effectively. However, this could also be attributed to

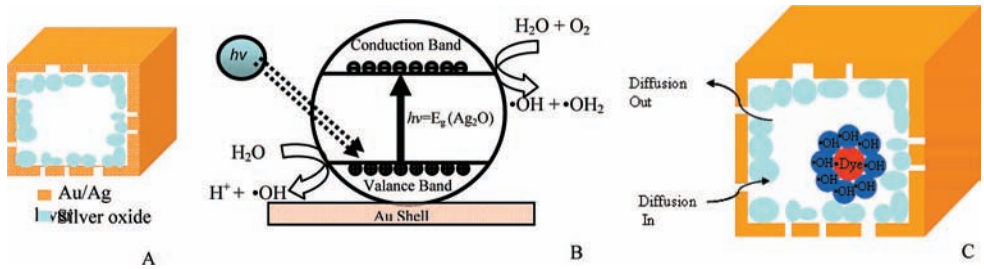

Figure 6. Schematic diagrams of (A) the oxygen-treated gold nanocage; (B) the photochemical generation of hydroxyl radical by silver oxide; (C) pores in the walls allowing solution to diffuse into the cavity where photodegradation takes places. When the size of the cage reaches a certain size, it could create a cage effect that confines the hydroxyl radicals inside the cavity.

the high surface coverage of the capping material to the external surface of the solid cube, which prevents molecular species from reacting with the surface. However, the reaction rate of the framelike AuNCs is not relatively large either (under 0.012 min^{-1}), even though there are numerous pore channels on the walls for the reactants to diffuse inside the cavity. In this case, the determining factor is the small Ag_2O surface area inside the cavity. In preparation of framelike AuNCs, hollow structures and pores are routinely produced. While this results in the formation of large pore channels, it also causes the decrease in the silver layers on the inner surface areas. This insufficient surface area of silver oxides could be the reason for the low activity of framelike AuNCs.

Therefore, achieving the optimum reaction rate requires (1) that there be a high surface area of Ag (which is oxidized to Ag_2O) on the inner wall of the cage to generate sufficient hydroxyl radicals, (2) that the channel (pore) sizes are sufficiently large enough to allow the reactants and products to diffuse into and out of the cavity but small enough to keep the radical steady state concentration high, and (3) that the cavity size inside the cage is appropriately sized to allow for an optimum collision rate between the reactants. When the pore sizes and surface area of silver oxide achieve a good balance, the cavity forms a "cage effect", meaning that the dye molecules could be caged by surrounding hydroxyl radicals and undergo a large number of collisions per unit time to enhance the reaction rate (Figure 6C). In our case, the cavity size of 75 nm AuNCs results in a reaction rate of 0.034 min^{-1}, which is twice as large as the rate with our other AuNCs catalysts.

Quantitative comparison can be made with other non-nanocage oxide catalysts, such as TiO_2[14] and ZnO.[15] The specific reaction rate constant is 0.034, 0.040, and 0.010 min^{-1} for the AuNCs, TiO_2,[14] and ZnO,[15] respectively. The reaction rate constant of TiO_2 is larger than that of AuNCs. However, the concentration of the catalysts used in TiO_2 (0.3 g/100 mL) is 15 times larger than that used in our experiment (0.02 g/100 mL). Furthermore, the strength of lamp used in the TiO_2 experiment is 500 W, while that used in our system is only 50 W. Thus one could conclude that the Ag_2O within the cavity of the AuNCs seems to be a more efficient photocatalyst. The explanation for the extremely high activity of the AuNCs is that it has an optimum balance of the three properties listed above, namely, a cavity with high Ag concentrations with pore sizes that allow the reactants and products to diffuse in and out without restrictions while confining the reactants in a small region that optimizes the collision frequency with hydroxyl radicals. The surface area of the silver oxides, pore channel sizes, and cavity sizes seem to be the crucial factors that determine the AuNCs activity, and these three factors can be easily tuned by the galvanic synthetic method to allow for the largest enhancement of the nanoreactor.

Acknowledgment. We would like to thank NSF support under Grant No. NSF CHE 0554668. We also thank Mr. Christopher Tabor for assistance in revising this manuscript.

References and Notes

(1) Li, Y.; Kunitake, T.; Fujikawa, S. *J. Phys. Chem. B* **2006**, *110*, 13000.
(2) Ng, Y. H.; Ikeda, S.; Harada, T.; Higashida, S.; Sakata, T.; Mori, H.; Matsumura, M. *Adv. Mater.* **2007**, *19*, 597.
(3) Yin, Y. D.; Rioux, R. M.; Erdonmez, C. K.; Hughes, S.; Somorjai, G. A.; Alivisatos, A. P. *Science* **2004**, *304*, 711.
(4) Su, F. B.; Lee, F. Y.; Lv, L.; Liu, J. J.; Tiax, X. N.; Zhao, X. S. *Adv. Funct. Mater.* **2007**, *17*, 1926.
(5) Zhou, S. H.; Varughese, B.; Eichhorn, B.; Jackson, G.; Mcllwrath, K. *Angew. Chem., Int. Ed.* **2005**, *44*, 4539.
(6) Chen, J.; Wiley, B.; Li, Z.; Campbell, D.; Saeki, F.; Cang, H.; Au, L.; Lee, J.; Li, X.; Xia, Y. *Adv. Mater.* **2005**, *17*, 2255.
(7) Lee, J.; Park, J. C.; Song, H. *Adv. Mater.* **2008**, *20*, 1523.
(8) Sun, Y.; Xia, Y. *Science* **2002**, *298*, 2176.
(9) Sun, Y.; Mayers, B.; Xia, Y. *Adv. Mater.* **2003**, *15*, 641.
(10) Cobley, C. M.; Campbell, D. J.; Xia, Y. N. *Adv. Mater.* **2008**, *20*, 748.
(11) Sun, Y.; Mayers, B.; Xia, Y. *Nano Lett.* **2002**, *2*, 481.
(12) Hoffmann, M. R.; Martin, S. T.; Choi, W.; Bahneman, D. *Chem. Rev.* **1995**, *95*, 69.
(13) Hachem, C.; Bocquillon, F.; Zahraa, M. B. *Dyes Pigments* **2001**, *49*, 117.
(14) Lin, X.; Huang, T.; Huang, F.; Wang, W.; Shi, J. *J. Phys. Chem. B* **2006**, *110*, 24629.
(15) Wu, J.; Tseng, C. *Appl. Catal., B* **2006**, *66*, 51.
(16) Rehren, F.; Muhler, M.; Bao, X.; Schlogl, R.; Ertl, G. *Z. Phys. Chem., Bd.* **1991**, *174*, 11.
(17) Strehlow, W. H.; Cook, E. *J. Phys. Chem. Ref. Data* **1973**, *2*, 163.
(18) Skrabalak, S. E.; Au, L.; Li, X.; Xia, Y. *Nat. Protocols* **2007**, *2*, 2182.
(19) Sun, Y.; Xia, Y. *Nano Lett.* **2003**, *3*, 1569.
(20) Lu, X.; Au, L.; McLellan, J.; Li, Z.; Marquez, M.; Xia, Y. *Nano Lett.* **2007**, *7*, 1764.
(21) Banerjee, S.; Maity, A. K.; Chakravorty, D. *J. Appl. Phys.* **2000**, *87*, 8541.
(22) Yin, Y.; Li, Z.; Zhong, Z.; Byron, G.; Xia, Y.; Venkateswaran, S. *J. Mater. Chem.* **2002**, *12*, 522.
(23) Kapoor, S. *Langmuir* **1998**, *14*, 1021.
(24) Chen, M.; Wang, L.; Han, J.; Zhang, J.; Li, Z.; Qian, D. *J. Phys. Chem. B* **2006**, *110*, 11224.
(25) Watehouse, G. I.; Bowmaker, G. A.; Metson, J. B. *Phys. Chem. Chem. Phys.* **2001**, *3*, 3838.
(26) Pettinger, B.; Bao, X.; Wilcock, I.; Muhler, M.; Schlogl, R.; Ertl, G. *Angew. Chem., Int. Ed. Engl.* **1994**, *33*, 85.
(27) Comparelli, R.; Fanizza, E.; Curri, M. L.; Cozzoli, P. D.; Mascolo, G.; Passino, R.; Agostiano, A. *Appl. Catal., B* **2005**, *55*, 81.
(28) Bahr, Y.; Mahmoud, M. A. *J. Phys. Chem. Solids* **2007**, *68*, 413.
(29) Braden, D. A.; Parrack, E. E.; Tyler, D. R. *Coord. Chem. Rev.* **2001**, *211*, 279.

JP811014U